Understanding lattice thermal conductivity in thermoelectric clathrates: A density functional theory study on binary Si-based type-I clathrates

Holger Euchner,[1] Stéphane Pailhès,[2] Valentina M. Giordano,[2] and Marc de Boissieu[3]
[1]*Helmholtz Institut Ulm, Helmholtzstrasse 11, D-89081 Ulm, Germany*
[2]*Institute of Light and Matter, UMR5306 Université Lyon 1-CNRS, Université de Lyon 69622 Villeurbanne cedex, France*
[3]*Science et Ingénierie des Matériaux et Procédés, Grenoble Alpes University, CNRS, Grenoble INP, 38000 Grenoble, France*

(Received 12 September 2017; revised manuscript received 15 December 2017; published 8 January 2018)

Despite their crystalline nature, thermoelectric clathrates exhibit a strongly reduced lattice thermal conductivity. While the reason for this unexpected behavior is known to lie in the peculiarities of the complex crystal structure and the interplay of the underlying guest-host framework, their respective roles are still not fully disentangled and understood. Our *ab initio* study of the most simple type-I clathrate phase, the binary compound Ba_8Si_{46} and its derivatives $Ba_{8-x}Si_{46}$ seeks to identify these mechanisms and provides insight into their origin. Indeed, the strongly decreased lattice thermal conductivity in thermoelectric clathrates is a consequence of a reduction of the acoustic phonon bandwidth, a lowering of the acoustic phonon group velocities, and the amplification of three-phonon-scattering processes. While the complexity of the crystal structure is demonstrated not to be the leading factor, the reasons are manifold. A modified Si-Si interaction causes a first decrease of the sound velocity, whereas the presence of flat Ba modes results in an additional lowering. These modes correspond to confined Bloch states that are localized on the Ba atoms and significantly increase the scattering phase space and, together with an increased anharmonicity of the interatomic interactions, strongly affect the phonon lifetimes.

DOI: 10.1103/PhysRevB.97.014304

I. INTRODUCTION

During recent years, the search for high performance thermoelectric materials with low thermal conductivity has been a major field of research. An efficient strategy for the development of robust thermoelectric materials with intrinsically low lattice thermal conductivity was achieved through phonon engineering in structurally complex materials [1–4]. Intermetallic clathrates are a class of structurally complex crystalline materials that combines a low lattice thermal conductivity of about 1 to 2 W/mK at 300 K with good electron mobility, thus making them promising candidates for thermoelectric applications [5,6]. One of the prominent features of these materials lies in their complex crystal structure, containing a large number of atoms that are organized in polyhedral cages. These cages form a covalent framework of four-bonded atoms (mostly group-14 elements) in which usually alkaline or alkaline-earth metals are entrapped [6,7]. The overall stability of intermetallic clathrates as well as their electrical properties can be fully understood in terms of the so-called Zintl-Klemm or charge balance rule [8,9].

The microscopic mechanism at the origin of their low thermal conductivity on the other hand—especially the difference of about two orders of magnitude between the thermal conductivity of diamond Si and Si-based clathrates as well as a sizable variation induced by changes in the electronic carrier concentration—is still under debate, specifically with respect to the roles of filler atoms and cage structure. Experiments and *ab initio* calculations on different clathrate phases point towards a strong hybridization of acoustic and low-energy optical phonon modes over an extended energy range [11–13]. These characteristic low-lying optical phonon modes that are evidenced in clathrates or skutterudites arise from vibrations of the entrapped guest atoms and frequently are termed rattling modes. They, however, coherently couple to the host framework and are well described within the harmonic approximation [11,12,14]. The hybridization of acoustic modes with these low-energy optical modes results in the bending of the acoustic dispersion, which in combination with a lowering of the sound velocity, yields a significant reduction of the acoustic bandwidth in thermoelectric clathrates. Moreover, the vibrational nature of acoustic phonon modes that are affected by the hybridization is changed from propagative to confined or localized Bloch states [11–13], similar to what is observed in disordered materials [15], quasicrystals [16–18], or nanostructured materials [19].

Apart from changes in dispersion and vibrational nature, the phonon lifetime—a quantity that is limited by anharmonic scattering processes—determines the lattice thermal conductivity. Experimentally, within the limits of the instrumental resolution of traditional inelastic-scattering experiments, no significantly increased anharmonic phonon-phonon scattering and hence no strongly reduced phonon lifetimes have so far been detected in clathrates [11,12]. A recent neutron spin-echo experiment reported the first direct measurement of phonon lifetimes in the Ge-based clathrate $Ba_{7.81}Ge_{40.67}Au_{5.33}$ and concluded that the thermal transport is dominated by low-energy acoustic phonons with long mean free paths, extending to at least 20 unit cells at 300 K [20]. Thus, the thermal transport in complex crystalline clathrates boils down to essentially the propagation of heat-carrying acoustic phonons [3,11,12,20], confined in a small energy range of a few meV, as previously suggested for complex dielectrics [21–23].

Consequently, the scattering processes which control the lifetimes of acoustic phonons remain to be understood. One unavoidable scattering channel is given by three-phonon processes, which can be mapped by current state-of-the-art *ab initio* calculations [24,25]. It formerly was suggested [26] and more recently confirmed by *ab initio* calculations [27–29] that the nondispersive low-energy optical phonons of complex guest-host materials open new paths for Umklapp scattering of heat-carrying acoustic phonons by multiphonon processes.

Despite these recent advances in experiment and theory, improving the way we picture thermal transport in thermoelectric clathrates, the situation is still unclear, and a better understanding of the underlying mechanisms is needed. To disentangle the different aspects that contribute to the lowering of the lattice thermal conductivity, in this paper we present a first-principles study in a series of $Ba_{8-x}Si_{46}$ compounds with different degrees of Ba filling. For this model system—comprising derivatives of the structurally simplest binary type-I clathrate [6,30]—we demonstrate that the covalent cage structure is not the main factor of the changing lattice dynamics and thermal transport between diamond Si and $Ba_{8-x}Si_{46}$. The presence of the Ba-guest atoms and the changing electronic configuration of the cages play a major role for the reduction of the acoustic energy bandwidth on the lowering of the phonon group velocities and on the enhancement of the multi-phonon-scattering processes.

II. COMPUTATIONAL MODELING

Ba_8Si_{46} is the structurally simplest binary type-I clathrate [6,30] and therefore was chosen as a model system for our computational study. Due to the framework not showing significant traces of disorder, related to the fact that no transition metals are necessary to stabilize the host framework [8], this phase is a perfectly suited candidate for studying various aspects of the guest-host interaction and its consequences for the thermal conduction. Moreover, recent *ab initio* studies on the lattice dynamics of this compound [11] show excellent agreement with experimental results. Especially the problem of a quite significant mismatch between experimental and calculated acoustic mode dispersions, which is evidenced in Ge-based clathrates [12,31], is not observed for Ba_8Si_{46}. This strongly indicates that, in the case of Ba_8Si_{46}, electronic structure methods are capable of capturing the important features accurately. Figure 1 depicts the unit cell of Ba_8Si_{46}, which is built up from two small (dodecahedral) and eight large (tetrakaidecahedral) Ba-encapsulating Si cages that form the Si-based host framework. To gain insight into the lattice dynamics of Si-based type-I clathrates, a series of $Ba_{8-x}Si_{46}$ model structures with different degrees of Ba filling was investigated computationally.

For our paper, we have used the periodic density functional theory code VASP for the optimization of different $Ba_{8-x}Si_{46}$ structures as well as for the determination of second- and third-order force constants, necessary for the investigation of lattice-dynamical properties. The calculations were conducted using the projector augmented-wave method to account for electron-ion interaction, whereas the general gradient approximation in the formulation of Perdew and Wang was applied to describe exchange and correlation. All structures were optimized with respect to volume and atomic position using an energy cutoff of 500 eV and a $5 \times 5 \times 5$ Γ-centered k-point mesh. The same settings were used for the determination of the force constants, which were obtained by introducing finite displacements into the ground-state structures [see the Supplemental Material (Ref. [10]) for further details].

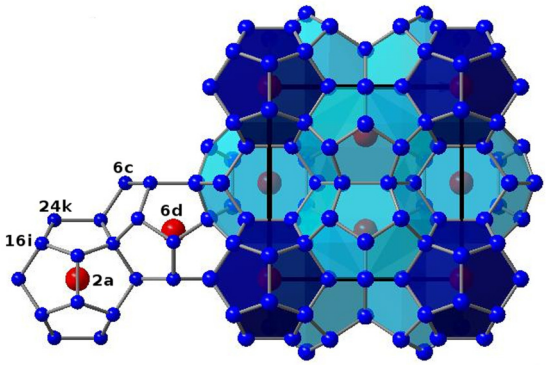

FIG. 1. Structure of Ba_8Si_{46}. Structure of the type-I clathrate Ba_8Si_{46}, with face sharing $BaSi_{20}$ and $BaSi_{24}$ cages as building units. Si atoms are depicted in blue, Ba atoms are depicted in red, whereas the black square in the background shows the dimensions of the unit cell. Moreover, the different Wyckoff sites are marked by the corresponding labels. Further structural details are given in Table SI1 of the Supplemental Material (Ref. [10]).

The harmonic force constants then were used to calculate dispersion curves, density of states (DOS), participation ratio (PR), and two-phonon-scattering phase-space $W_q^{\pm}$ for phonon absorption/emission. Lattice thermal conductivity and phonon lifetimes on the other hand were obtained in the framework of the Boltzmann transport equation by including the anharmonic force constants. For both, the determination of harmonic and anharmonic properties, the ALAMODE code [25,27] was utilized.

III. RESULTS

To disentangle the effects that are responsible for the large changes in thermal conductivity, when going from pure diamond silicon to the binary clathrate Ba_8Si_{46}, initially three different model systems have been studied. First, the covalent Si_{46} network without guest atoms is investigated. In a next step, the Si_{46} network without guest atoms but with the Si-Si interaction potential obtained from the Ba_8Si_{46} clathrate phase is modeled. This system, which in the following will be referred to as BaSi-Si_{46}, allows us to study the impact of Ba on the electronic structure and the Si-Si interaction potential. Finally, in order to isolate purely electronic effects, a charged Ba-free Si_{46} network, referred to as charged-Si_{46}—with the additional charge corresponding to two electrons per cage (i.e., 16 electrons in the unit cell)—was studied. This scenario mimics a Si_{46} framework that has accepted two valence electrons from each encaged Ba atom with subsequent removal of the Ba ions. In the next step, the effect of gradually filling the cages of an empty Si_{46} framework was investigated. All changes in the phonon spectra, when going from the pure diamond structure

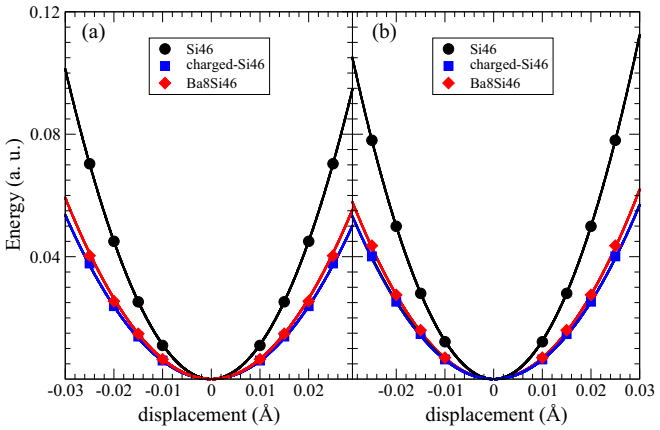

FIG. 2. Si interaction potential. Potential energy of a Si atom at the 6*c* site (0.25,0,0.5), in Si_{46}, charged-Si_{46}, and Ba_8Si_{46} for the two-symmetry nonequivalent directions. The potential energies are shown along the direction [100] in (a) and along the direction [010] in (b). The symbols are calculated for the corresponding displacements. The solid lines represent the harmonic potential as obtained for displacements of 0.02 Å, corresponding to those used for the phonon calculations.

to clathrate phases, have to be related to the organization of a large number of atoms in a network of cages, the mass effect of the heavy Ba atoms, and the changes in the electronic structure caused by the negative charge that is added to the covalent framework by the electropositive Ba ions.

Interaction potential and phonon dispersion

The potential energies of the silicon atoms on the Si (6*c*) site (see Fig. 1) with respect to displacements out of the equilibrium position were determined for Si_{46}, charged-Si_{46}, and Ba_8Si_{46}, following the symmetry nonequivalent directions, i.e., along [100] and [010], and are shown in Figs. 2(a) and 2(b), respectively. They were obtained by determining the restoring forces for different displacement amplitudes. The potentials of the additional Si sites (Si-24*k* and Si-16*i*) are similar to that of the Si (6*c*) site and are therefore only shown in the Supplemental Material [10]. First, in all directions probed, the potential energies of Si follow a quadratic dependence on the displacements in agreement with previous works in clathrates showing that, despite the complexity and the large open spaces in the cages, the potential energies of the host and guest atoms are harmonic over a wide range of displacements [31,32]. Second, the potential shapes, corresponding to the three silicon sites, are affected strongly when Si_{46} and charged-Si_{46} are compared. The additional charge clearly results in a significant weakening of the Si-Si interaction whereas the differences between the potentials in charged-Si_{46} and Ba_8Si_{46}, induced by the actual presence of the Ba atoms inside the cages, are negligible. In fact, the evidenced softening of the Si interaction potential can be easily understood by investigating the electronic density of states of the different compounds (see the Supplemental Material [10]). In charged-Si_{46} and Ba_8Si_{46} the additional electrons fill up the antibonding states which are empty in the case of the covalent Si_{46} framework. Consequently, while covalent Si_{46} is an insulator, the filling of the antibonding states in charged-Si_{46} and Ba_8Si_{46} makes these two compounds metallic and weakens the Si-Si interaction. Thus, the interaction potential of the silicon atoms in Ba_8Si_{46} is strongly different from the one of covalent Si_{46}, which is mainly due to the differences in electronic configuration induced by electron transfer from encapsulated Ba atoms to the Si_{46} framework.

The phonon-dispersion curves for Si_{46}, BaSi-Si_{46}, and charged-Si_{46} were determined using the above-described methodology and are depicted in Fig. 3. Similarly, the phonon dispersions obtained after the introduction of one single Ba atom into the Si framework either on the Wyckoff site 2*a* or on the Wyckoff site 6*d* as well as for the completely filled Ba_8Si_{46} are depicted in Figs. 3(d)–3(f) (further configurations with different Ba contents are shown in the Supplemental Material [10]). For all six cases the dispersion curves were calculated along the Γ-*X*-*M*-Γ-*R* pathway, connecting the corresponding high-symmetry points in the Brillouin zone (BZ) and following the reciprocal space directions [100], [010], [110], and [111].

The phonon-dispersion curves of charged-Si_{46} and BaSi-Si_{46} frameworks show very similar behavior and are remarkably different from covalent Si_{46}, which is due to the changes in the interaction potential discussed above. In the latter one, the longitudinal acoustic (LA) and transverse acoustic (TA) phonon modes follow a perfectly linear dispersion from the zone center to the borders of the BZ. While the LA (TA) modes reach an energy of about 15 (9) meV at the *X* point, they amount to 17 (11) meV at the *M* point. The main difference with respect to the other Si_{46} frameworks is a significant decrease of about 5 meV in the phonon energies at the BZ edges (*X*, *M*, and *R* points) in charged-Si_{46} and BaSi-Si_{46}, thus drastically reducing the energy bandwidth available for acoustic phonons. As suggested in Ref. [12], the acoustic bandwidth can be quantified by a cutoff energy E_{cut}, thus giving a measure for the energy range accessible for acoustic phonons. This cutoff energy is closely related to both the van Hove singularities that arise from the flattening of the acoustic dispersions at the borders of the BZ and the nondispersive low-energy optical phonon branches [11,12,33]. Concomitant with the reduction of the acoustic bandwidth, several theoretical studies have highlighted the changing vibrational character of the heat-carrying acoustic phonons induced by the strong hybridization with the low-energy guest vibrations by considering the phonon PR [11,13,27]. The PR is an indicator for the character of a phonon mode (see the Supplemental Material [10]) such that a PR close to 1 is typical for an acousticlike excitation, whereas a PR below about 0.3 points to a strongly confined mode, here essentially localized on the Ba atoms, which will not significantly contribute to the heat transport. It is important to note that the term localized is not to be understood in the sense of an eigenstate that shows an exponential decay of the vibrational amplitude with increasing distance from the center of the mode. In this context localized means a Bloch state that is confined to a certain part of the structure and the periodic repetitions of this part, giving a special character to such a phonon mode. In clathrates, this scenario has to be distinguished from the one of the exponentially decaying non-Bloch states that are evidenced for off-center systems [33,34]. Thus, for an unambiguous definition of the acoustic limit and the corresponding cutoff energy E_{cut}, the PR is suited perfectly. In the following, we define the acoustic limit as the

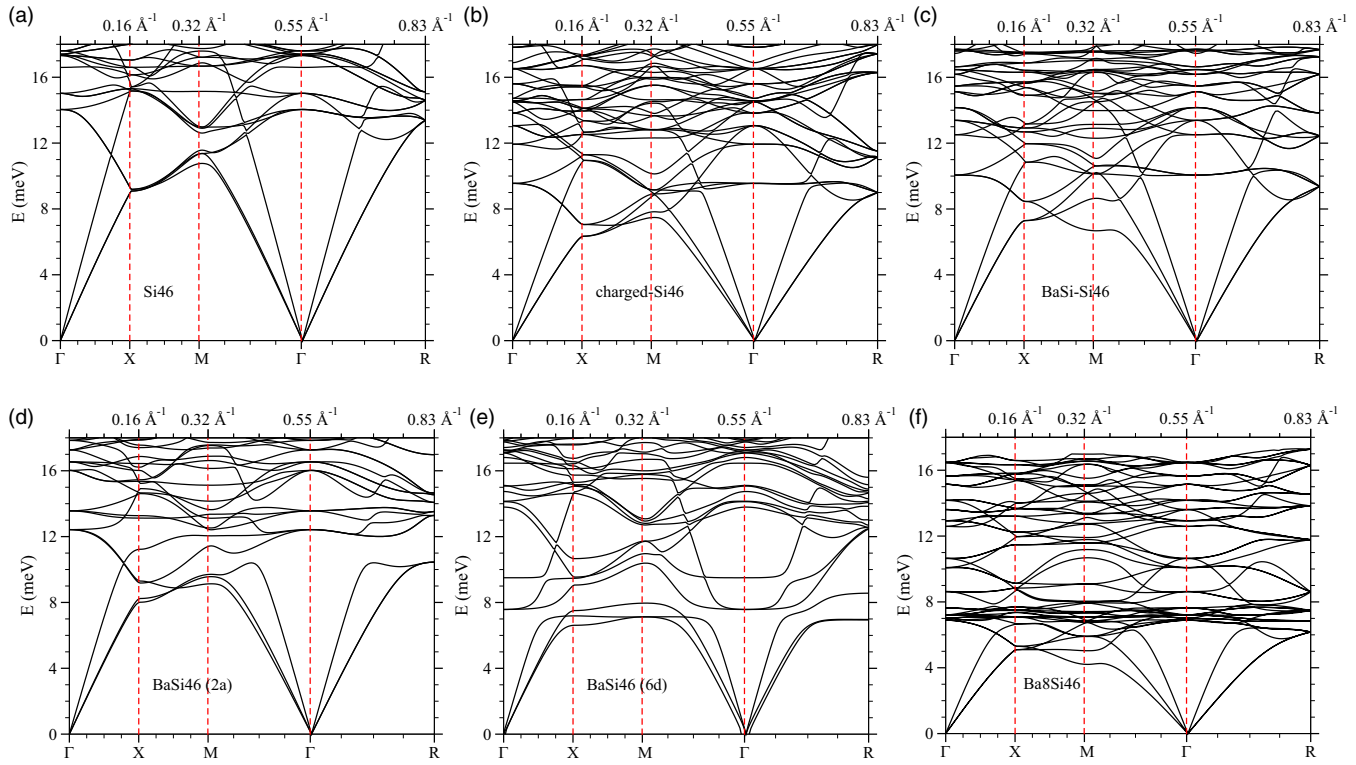

FIG. 3. Phonon dispersions along Γ-X-M-Γ-R. All panels show the phonon dispersions along the same pathway, connecting the high-symmetry points Γ-X-M-Γ-R. The corresponding phonon wave vectors in Å^{-1} are reported on the top axis. The top panels (a)–(c) show the dispersion curves of Si_{46} (left), charged-Si_{46} (middle), and BaSi-Si_{46} (right), respectively. The bottom panels (d)–(f) depict the dispersion curves of $BaSi_{46}$ with one Ba at a 2a site (left), $BaSi_{46}$ with one Ba at a 6d site (middle), and Ba_8Si_{46} (right). The vertical dashed lines in all panels indicate the positions of the high-symmetry points.

minimum energy at which the PR of any acoustic mode drops for the first time below a value of 0.5 (see the Supplemental Material [10] for further details). The resulting cutoff energies $E_{\rm cut}$ are given in Table I and provide an estimate of the energy range available for acoustic phonons, which in fact may be used to define a modified Debye temperature, correctly describing the lattice dynamics of complex materials [35].

TABLE I. Sound velocities and acoustic limit. The sound velocities (in m s^{-1}) of the LA dispersion $v^s_{\rm LA}$ and the two TA dispersions $v^s_{TA1,2}$ along the direction Γ-M are reported. They allow for determining the Debye sound velocity, defined as $3v_D^{-3} = v_{TA1}^{-3} + v_{TA2}^{-3} + v_{\rm LA}^{-3}$. Moreover, for each system, the cutoff energy $E_{\rm cut}$ (in meV), the corresponding modified Debye temperature $\Theta_D = E_{\rm cut}/k_B$ (in Kelvin), and κ_L (in W/mK) at a temperature of 100 K are given.

Compound	v_{TA1}	v_{TA2}	$v_{\rm LA}$	v_D	$E_{\rm cut}$	Θ_D	κ_L
Si_{46}	4608	4773	8075	5202	15.1	175.2	291.2
Charged-Si_{46}	3158	3581	6395	3740	9.0	104.4	31.3
BaSi-Si_{46}	3649	4288	6730	4346	10.8	125.3	15.7
$BaSi_{46}$ (2a)	4177	4543	7583	4827	9.43	109.4	44.5
$BaSi_{46}$ (6d)[a]	4368	4406	7330	4854	6.18	71.7	2.6
Ba_8Si_{46}	2329	2999	5496	2906	5.24	60.7	1.1

[a]The $v^s_{TA1,2}$ and $v^s_{\rm LA}$ in the case of $BaSi_{46}$ (6d) had to be determined at a distance of ∼0.02 Å^{-1} from the M point due to a slight instability.

When comparing $E_{\rm cut}$ of the empty Si_{46} frameworks, we find that up to 40% of the phase space available for acoustic phonons is suppressed in the charged-Si_{46} and BaSi-Si_{46} framework as compared to the case of covalent Si_{46}. Obviously, this drastically affects the thermal transport, which is known to be dominated by acoustic phonon modes. Furthermore, this strong reduction of the phase space is accompanied by a pronounced bending of the acoustic phonon dispersions and consequently a strong decrease in the phonon group velocities for all polarizations (TA and LA) and all directions. These changes also contribute to reduce the thermal conduction by opening new channels for multiphonon scattering. Finally, the optical spectra are clearly shifted towards lower energies, resulting in the appearance of almost dispersionless modes at about 10 meV around the Γ point (see along M-Γ-R). These modes affect the heat capacity and contribute to large deviations in its temperature dependence from the usual Debye T^3 dependence. On the other hand, due to their small group velocities, these modes do not significantly contribute to the lattice thermal conductivity, however, they open scattering channels with the acoustic phonons and thus indirectly damage the heat conduction as discussed below.

The phonon dispersions reported in Figs. 3(d)–3(f) show the effect of filling the cages by Ba atoms. The impact of a Ba atom in a small cage (Ba-2a site) is clearly less significant than that of a Ba atom in a large cage (Ba-6d site). In fact, the small cage Ba exerts its main influence on phonon modes with energies above 10 meV, whereas the large cage Ba strongly

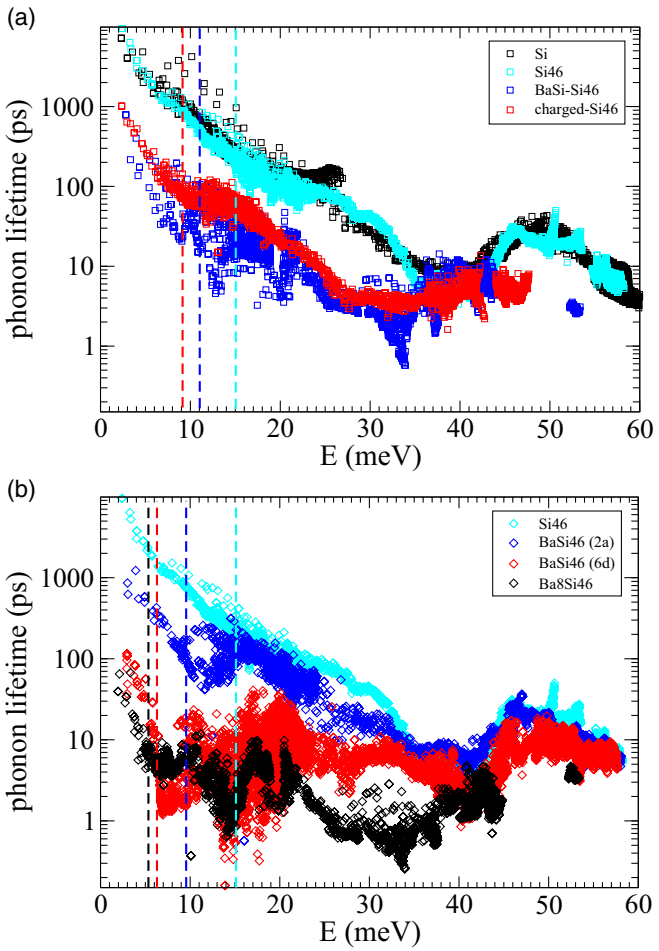

FIG. 4. Phonon lifetimes. (a) Phonon lifetimes (in picoseconds) for diamond Si (black), covalent Si_{46} (cyan), charged-Si_{46} (blue), and BaSi-Si_{46} (red) at a temperature of 100 K. (b) Phonon lifetimes of $BaSi_{46}$ with one Ba atom at the 2*a* (blue) site and one at the 6*d* (red) site, respectively, as compared to covalent Si_{46} (cyan) and Ba_8Si_{46} (black) at a temperature of 100 K. The dashed lines indicate the cutoff energies of the corresponding compound (see Table I).

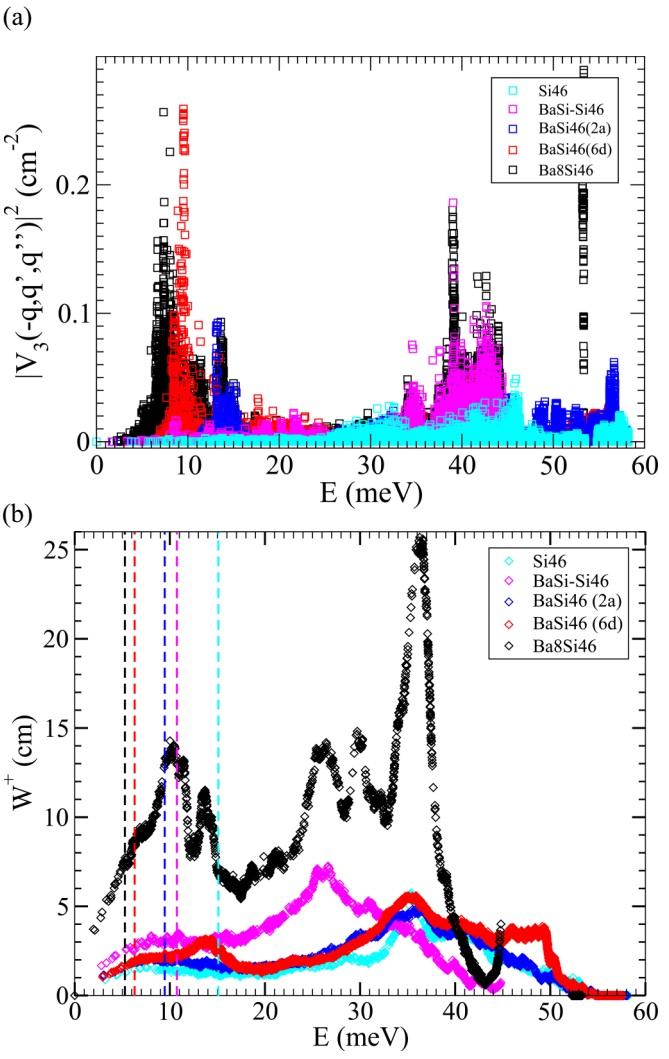

FIG. 5. Phonon anharmonicity. (a) Amplitude of the anharmonic matrix elements of the three-phonon scattering processes $|V_3(q,q',q'')|^2$ for TA acoustic modes at $q = (0,0,0.1)$ and (b) the all-phonon energy and momentum-conservation phase-space (W^+) at a temperature of 100 K for $BaSi_{46}$ with Ba in a small cage (blue) and a large cage (red) as compared to Si_{46} (cyan), BaSi-Si_{46} (magenta), and Ba_8Si_{46} (black). The dashed lines indicate the cutoff energies of the corresponding compound (see Table I).

alters the LA and TA phonon dispersions at lower energies. A comparison with the dispersion curves in BaSi-Si_{46} [Fig. 3(c)] points to the Ba atoms as a reason for the pronounced bending and flattening of the acoustic dispersions close to the borders of the BZ at the X, M, and R points thus yielding a decrease in the LA and TA group velocities and the corresponding sound velocities as reported in Table I. Moreover, the energies of the optical phonons at the Γ point are strongly decreased by almost 2 meV leading to a reduction of the available phase space for acoustic phonons as shown by the values of E_{cut} reported in Table I.

While the increasing charge transfer (going along with the gradual filling of the cages) and the corresponding changes in the Si-Si interaction result in a depression of the phonon spectra as can be seen from the dispersion curves [see Figs. 3(a)–3(c)] and especially from the phonon DOS (see Fig. 4 in the Supplemental Material [10]), the filling of the clathrate framework introduces additional degrees of freedom and consequently additional phonon modes. These extra modes are responsible for the further depression of the acoustic regime and the additional lowering of the sound velocity, similar to what is found in skutterudites [28,29]. This is again nicely seen from the density of states plots in the Supplemental Material [10] where it is clearly visible that the essential differences between BaSi-Si_{46} and Ba_8Si_{46} stem from the additional modes that are introduced below about 10 meV (see Figs. 4 and 5 in the Supplemental Material [10]). Finally, with the filling of the cages, the Ba potential is getting softer along one direction. This mainly affects Ba modes with strong components perpendicular to the hexagonal plane of the surrounding cage and may shift the latter ones to somewhat lower energies (see the Supplemental Material [10]).

Anharmonicity and phonon lifetimes

In Figs. 4(a) and 4(b), the individual phonon lifetimes, obtained by sampling the reciprocal space (see the Supplemental Material [10] for details), resulting from the three-phonon scattering processes for the different compounds discussed above are depicted. The phonon lifetimes were calculated for a temperature of 100 K and are shown for the whole energy spectrum. The effects of cage structure and electronic configuration of the silicon network are discussed with the support of panel (a), whereas the impact of filling the cages by Ba atoms is analyzed with respect to panel (b).

The comparison of diamond Si and covalent Si_{46} in Fig. 4(a) shows that the overall energy dependence of their phonon lifetimes is quite similar. These similarities in phonon lifetime are in good agreement with the study of Härkönen and Karttunen [36] where a comparison between diamond Si and empty type-II and type-VIII frameworks is shown. Moreover, similar conclusions for Ge_{46} and diamond Ge were obtained from molecular dynamics (MD) simulations in the context of the linear-response theory [37].

These similarities between the phonon lifetimes in diamond Si/Ge and covalent Si_{46}/Ge_{46} disagree with the recent conclusion of a large decrease in the phonon lifetime in Si_{46} compared to diamond Si [38]. However, in Ref. [38] the evidenced decrease in the phonon lifetimes in Si_{46} may be traced back to the introduction of a scaling factor in the definition of their Debye temperature. This factor is supposed to account for the complexity of the structure and includes the number of atoms per unit cell. Consequently, this decrease in phonon lifetime is somewhat artificial and originates in the increased structural complexity of Si_{46} as compared to diamond Si, but it is not intrinsic to the lifetime of the heat-carrying acoustic phonons. In fact, with the above-suggested definition of a modified Debye temperature, with respect to the cutoff energy, the semiempirical model of Madsen *et al.* [38] would yield results in good agreement with our findings.

From our calculations, the only significant differences between the lifetimes in diamond Si and covalent Si_{46} are found in the intermediate-energy range from 40 to 50 meV where a faster decrease in the lifetime is evidenced in the case of Si_{46}. This actually indicates that the impact of the cage structure on the phonon lifetimes due to three-phonon-scattering processes is not the dominant factor for the reduced lattice thermal conductivity in clathrates. On the other hand, the phonon lifetimes in the charged-Si_{46} and the BaSi-Si_{46} framework are strongly reduced when compared to diamond Si and covalent Si_{46}. Especially, in the low-energy range below E_{cut}, the phonon lifetimes are roughly one order of magnitude smaller, ranging from 1 to 10 ps, whereas in case of covalent Si_{46} and diamond Si the 10-ps limit is only undershoot beyond 30 meV.

In the next step, the impact of Ba-guest atoms on the phonon lifetimes is visualized for $BaSi_{46}$ with one Ba atom in the small cage (Ba 2*a*) and for $BaSi_{46}$ with one Ba atom in the large cage (Ba 6*d*), respectively. From the phonon lifetimes as depicted in Fig. 4(b), it is clear that the insertion of a single Ba atom in a small cage leads to a significant reduction of the phonon lifetime with respect to covalent Si_{46}. The reduction occurs mainly in the acoustic energy range, below 10 meV, where the lifetimes decrease by roughly a factor of 5. In the high-energy limit, there are only marginal differences in comparison to Si_{46}. For $BaSi_{46}$ with a Ba atom in the large cage a tremendous decay of the lifetimes is observed below about 20 meV. Especially in the acoustic regime the lifetimes are about two orders of magnitude smaller than in diamond Si and Si_{46}. As will be discussed below, this tremendous decrease in phonon lifetime strongly affects thermal transport and confirms the important role of the Ba-dominated optical phonon branches—frequently referred to as rattling modes. These modes indeed are at the origin of the strong enhancement of the scattering of the acoustic phonons by means of three-phonon processes. Finally, the comparison of $BaSi_{46}$ and the fully occupied Ba_8Si_{46}, also see Fig. 4(b), shows a further decrease in the lifetimes with an increasing amount of Ba, consistent with a further enhancement of three-phonon processes. Indeed, for most energies, the phonon lifetimes in Ba_8Si_{46} lie below those of $BaSi_{46}$ with a filled large cage, yet, the most significant decrease is only visible in the intermediate-frequency range from 20 to 40 meV. These results agree with the large decrease in the phonon lifetimes obtained by *ab initio* calculations for the completely filled $Ba_8Ga_{16}Ge_{30}$ clathrate when compared to the empty $Ga_{16}Ge_{30}$ framework [27].

To further enlighten the origin of the decreasing phonon lifetimes, the two factors determining the strength of the three-phonon-scattering cross section, the anharmonic interaction strength and the phase space for energy and momentum conservation, were analyzed separately. The probability of a phonon q to be scattered in a three-phonon process with the phonons q' and q''—assuming that the necessary conditions, i.e., energy and momentum conservation are fulfilled—depends on the strength of the anharmonic interaction. This interaction strength is described by the matrix element $|V_3(q,q',q'')|^2$, which is directly related to the cubic force constants (see the Supplemental Material [10]). The energy- and momentum-conservation phase-space $W_q^{\pm}$, on the other hand, determines how frequently the conditions for a scattering event are met (see the Supplemental Material [10]). Thus, a low phonon lifetime can result either from a strong anharmonicity or from a large phase space with respect to the conservation laws.

To disentangle these two terms, we have calculated $|V_3(q,q',q'')|^2$ for scattering events that fulfill energy and momentum conservation for a TA phonon mode at $q = (0,0,0.1)$, see Fig. 5(a). The energies corresponding to this TA phonon mode of covalent Si_{46}, BaSi-Si_{46}, $BaSi_{46}$ (2*a*), $BaSi_{46}$ (6*d*), and Ba_8Si_{46} are 1.93, 1.70, 1.81, 1.79, and 1.19 meV, respectively, and thus far from the acoustic limit. In the low-energy part of the spectrum, the Ba-free systems Si_{46} and BaSi-Si_{46} behave rather similarly and show comparatively weak anharmonicity, see Fig. 5(a). Ba_8Si_{46} and $BaSi_{46}$ (6*d*) with one Ba in the large cage, on the other hand, show significant anharmonic interaction strength in the low-energy range below about 15 meV with the strongest intensity at about 7 and 9 meV, respectively. This clearly points to scattering processes involving the flat Ba-dominated modes that are observed in this energy range. For $BaSi_{46}$ (2*a*), the maximum anharmonic interaction strength lies between 12 and 15 meV, which corresponds essentially to scattering processes with the modes dominated by vibrations of the Ba atom in the small cage. In the intermediate-energy range, between 20

and 40 meV, the completely filled Ba_8Si_{46} clathrate shows strongly increased anharmonicity, whereas for $BaSi_{46}$ ($6d$) the intensity drops to a similar level as for $BaSi_{46}$ ($2a$) and covalent Si_{46}. Interestingly, for BaSi-Si_{46} we evidence a significantly increased anharmonicity in this intermediate-frequency range, being almost as strong as in the case of filled Ba_8Si_{46}. This again corroborates our previous findings that both, the change in the Si-Si interaction due to the charge transfer and the presence of Ba atoms at the $6d$ site contribute to the extraordinary lattice thermal conductivity of clathrates.

Moreover, to conclude on the respective impact of anharmonic interaction strength $|V_3(q,q',q'')|^2$ and the temperature-dependent phase space for phonon absorption W_q^+, the latter one is reported in Fig. 5(b). While the anharmonicity, observed for the TA mode, already is able to explain the qualitative changes in the phonon lifetimes of the investigated compounds, it has to be pointed out that the phase space for phonon absorption/emission is a further important source for the evidenced differences. As can be inferred from the phase space for phonon adsorption W_q^+, calculated at a temperature of 100 K as depicted in Fig. 5(b), this quantity also contributes to the reduction of the phonon lifetimes. In fact, there exists a large difference between unfilled and partially filled clathrates on one hand and completely filled clathrates on the other hand. The presence of the large number of dispersionless modes in the low-frequency range of Ba_8Si_{46} (see, e.g., the dispersion curves in Fig. 3 or the corresponding density of states in the Supplemental Material [10]) results in a considerable increase in available scattering channels, i.e., a strongly increased W_q^+ and thus decreasing phonon lifetimes. These findings agree nicely with previous results on skutterudites where the presence of flat dispersionless modes was shown to significantly enhance the number of scattering channels over the whole energy range [28,29] A difference from the case of skutterudites, however, is the fact that the increased three-phonon-scattering phase space alone is not enough to account for the decreasing phonon lifetimes. As shown above, the anharmonic interaction strength also is changing significantly from Si_{46} to Ba_8Si_{46}.

Lattice thermal conductivity

The experimentally measured room-temperature lattice thermal conductivities of Ba_8Si_{46} and its known ternary derivatives (Au, Cu, Al, and Ni-doped Ba_8Si_{46}) are on the order of 1 to 2 W/mK [11,39–43] thus lying in the typical range of thermal conductivities evidenced for similar materials. Interestingly, sizable variations of the lattice thermal conductivity, induced by changes in the electronic carrier concentration of the Si_{46} framework, are observed at room temperature and above in $Ba_8Cu_xSi_{46-x}$ [42] and in $Ba_8Al_xSi_{46-x}$ [43] which have been ascribed to electron-phonon-scattering processes. Moreover, a recent experimental investigation of the undoped $Ba_{7.2}Si_{46}$ reported a lattice thermal conductivity of about 6 W/mK at 300 K accompanied by the absence of the characteristic Umklapp peak. This rather high value and the evidenced temperature dependence were rather surprising in comparison to the previously mentioned ternary varieties and other type-I clathrates in general [9].

The herein chosen theoretical approach of applying the Boltzmann transport equation, limited to three-phonon processes, results in the well-known umklapp-related $1/T$ temperature dependence of the lattice thermal conductivity. For clathrates, this $1/T$ decay results in calculated lattice thermal conductivities on the order of 0.1 W/mK at room temperature. However, in clathrates, as well as in other cage-based materials, such low room-temperature thermal conductivities have never been observed. Moreover, a glasslike plateau frequently is measured in clathrates for a temperature range from about 40–300 K [6].

So far, there are no clear explanations for such discrepancies, but several origins may be thought of: First, the fact that, at the current level of theory, higher-order terms are neglected and normal processes are treated as resistive may play a role. The discrepancies may as well be an indication that two-phonon processes are involved, similar to the scenario in disordered systems. Finally, diffusive-type processes might also give a contribution to the thermal conductivity. From a theoretical point of view, an extension of the currently applied formalism to include higher-order phonon scattering would be needed in order to reproduce the deviations from the $1/T$ temperature dependence of the lattice thermal conductivity. Interestingly, a more realistic T dependence is evidenced in some classical MD simulations applying the Green-Kubo formalism [37,44] that in principle accounts for all phonon-scattering processes, thus also implying the importance of higher-order processes.

The calculated temperature dependence of the lattice thermal conductivity for the different compounds under investigation is reported in Fig. 6. At this point it is important to note once again that only three-phonon-scattering processes are considered within the presented computational approach. Due to the limitations of this approach, as discussed previously, the absolute values of thermal conductivity as well as the $1/T$ dependence do not correctly reproduce the experimental findings (see, e.g., Fig. 8 in the Supplemental Material [10]), but tendencies can nevertheless be predicted.

The lattice thermal conductivity of Si_{46} is quite close to the one of diamond Si, and in a large temperature range they differ by roughly a factor of 3 as can be inferred from Fig. 6(a). This simply reflects the fact that phonon dispersion and anharmonicity in the two systems are also very similar as discussed above. This corresponds well to the results of Härkönen and Karttunen [36] for empty type-II and type-VIII Si clathrates where a decrease in κ_L of about 38 and 31% as compared to diamond Si is reported at 350 K. This together with the qualitatively similar dispersion curves for the different clathrate structure types clearly indicate that the underlying mechanisms are similar. Furthermore, this finding confirms that the cage structure alone cannot be responsible for the two orders of magnitude difference in lattice thermal conductivity between diamond Si and the clathrate phase Ba_8Si_{46}. A first significant reduction of the lattice thermal conductivity, more than a tenfold decrease compared to Si, is achieved for charged-Si_{46} and BaSi-Si_{46}. As discussed above, the additional charge in the covalent Si framework drastically changes the interaction potential of the Si atoms, resulting in the evidenced strong decrease in the lattice thermal conductivity, see Fig. 6(a). The second significant reduction originates from the filling of the cages, especially from the Ba ($6d$) site as shown in Fig. 6(b). These results again are congruent with our expectations from previous sections. The Si_{46} framework with only one Ba atom

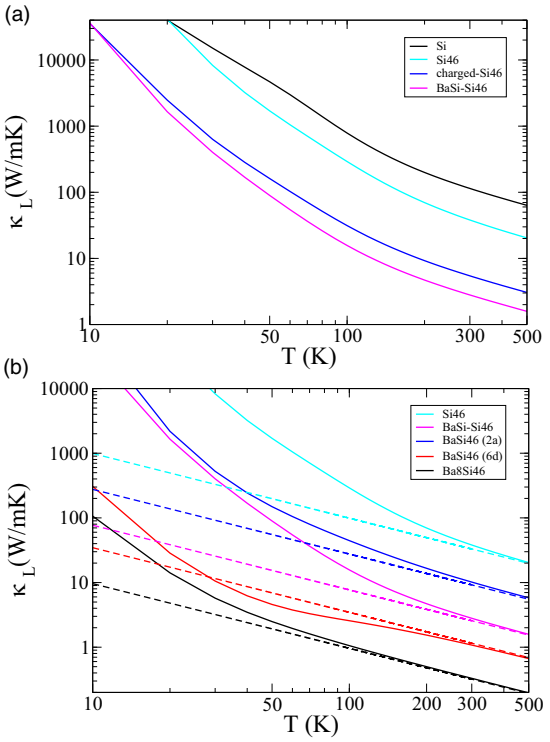

FIG. 6. Lattice thermal conductivity. (a) Lattice thermal conductivity κ_L, resulting from three-phonon processes in Si_{46} (black), BaSi-Si_{46} (red), and charged-Si_{46} (blue) as compared to diamond Si (cyan). (b) κ_L in Si_{46} (green), $BaSi_{46}$ with one Ba atom at the 6*d* Wyckoff site (red) and one Ba at the 2*a* site (blue) and BaSi-Si_{46} (cyan) as compared to Ba_8Si_{46} (black). The dashed lines show the corresponding $1/T$ dependences towards which the respective curves are converging.

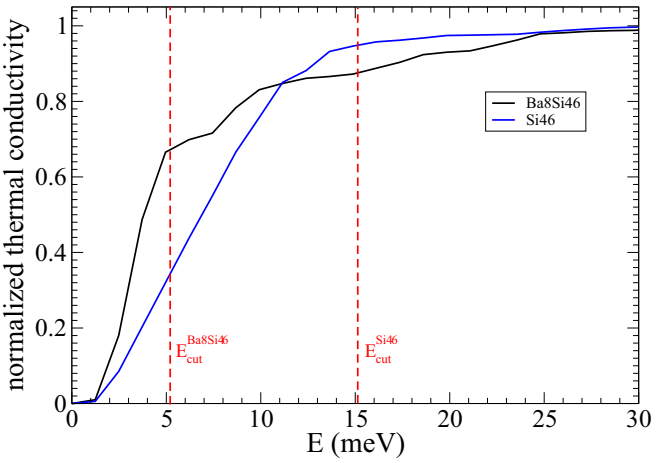

FIG. 7. Cumulative lattice thermal conductivity. Percentage of the thermal conductivity which is reached with respect to the energy range in Ba_8Si_{46} (black) and in Si_{46} (blue) for a temperature of 100 K. The red dashed lines indicate the cutoff energy E_{cut} which describes the limit of the acoustic regime as introduced previously.

at a 2*a* site shows a thermal conductivity that lies far above that one of the framework with one Ba atom at a 6*d* site. The completely filled framework shows a further decrease as compared to the Ba-6*d* case with κ_L decreasing below 1 for temperatures above ∼100 K. Interestingly, a comparison of Ba_8Si_{46} and two different Ba_7Si_{46} compounds shows equally low lattice thermal conductivity (see the Supplemental Material [10]) such that the lowest κ_L value may actually be found for a clathrate with not fully occupied cages. This means that the increased anharmonicity in the low-energy range (due to empty cages) may compensate the somewhat decreased phase space.

In Fig. 7 the frequency-integrated normalized spectral thermal conductivity, also called the cumulative thermal conductivity, of Ba_8Si_{46} and Si_{46} is shown for a temperature of 100 K. The cumulative thermal conductivity at a given energy E represents the contribution to the total thermal conductivity up to this energy. The dashed lines indicate the values of E_{cut}, given in Table I, the energies below which the acoustic phonon branches are well defined. The depicted comparison between Ba_8Si_{46} and Si_{46} shows that in both cases the thermal conductivity increases roughly linear up to E_{cut} where the curves then become significantly flatter. This behavior also nicely corroborates our definition of the acoustic limit. With respect to the total thermal conductivity, we find that for the filled clathrate almost 70% of the thermal conductivity at 100 K lie in the energy range between 0 and $E_{cut}^{Ba_8Si_{46}}$ (5.24 meV), whereas for the empty Si_{46} framework only about 35% of the thermal conduction stem from modes below $E_{cut}^{Ba_8Si_{46}}$. For the case of Si_{46} on the other hand, we find that at 100 K ($< E_{cut}^{Si_{46}}/k_B$) more than 90% of the thermal conductivity can be attributed to the acoustic regime, again pointing to the physical significance of the cutoff energy.

IV. DISCUSSION

Finally, from the comparison of empty frameworks and clathrates with different degrees of filling, we can conclude that the reduced thermal conductivity in intermetallic clathrates cannot only originate from the structural complexity of these phases. In fact, the structural complexity of the Si_{46} framework neither results in a significantly higher anharmonicity of the Si-Si interaction nor in an increased amount of scattering channels when compared to diamond Si. Over a wide temperature range and especially in the high-temperature limit, i.e., above the Debye temperature, the lattice thermal conductivity of Si_{46} is about three times lower than in Si. This difference can indeed be related to the crystal complexity factor, formerly introduced in complex dielectric materials [21–23]. In the case of Si_{46} with $N = 46$ atoms in the unit cell, this factor is $N^{1/3} \sim 3.5$. The quantitative agreement of this factor with the calculated differences implies that the acoustic phonon modes dominate the heat transport. This is in accordance with our finding that acoustic modes carry 90% of the heat in Si_{46}.

Beyond the crystal complexity, the decreased lattice thermal conductivity in the filled Si clathrates can be attributed to two main factors. First, there is a strongly altered Si-Si interaction potential which arises from the charge transfer to the Si_{46} framework as could be niecly shown with the comparison of Si_{46}, charged-Si_{46}, and BaSi-Si_{46}. This leads to a reduction of the sound velocity and the acoustic regime as can be seen from the differences in the cutoff energies of the respective

compounds. The second important contribution is directly related to the insertion of Ba at the 6*d* site, whereas the insertion of Ba at the 2*a* site only has a minor effect. Filling of a Ba (6*d*) site results in a further decrease in the sound velocity and shifts the acoustic limit down to almost 5 meV. In addition, occupying the Ba (6*d*) site results in a significantly increased anharmonicity in the low-energy limit. Together with the increasing scattering phase space, which is a consequence of the opening of further scattering channels due to flat Ba modes, this results in shorter phonon lifetimes, especially of the acoustic modes.

Thus, the most significant differences between the clathrate Ba_8Si_{46} and diamond Si are an increased anharmonicity, a drastic reduction of the phase space available for acoustic phonons, and the consequential reduction of the sound velocity. The latter can be quantified by comparing the Debye temperature in diamond Si, $\Theta_D^{\mathrm{Si}} \sim 700$ K, and the Debye temperature of Ba_8Si_{46} as defined from the cutoff energy given in Table I $\Theta_D^{\mathrm{Ba_8Si_{46}}} = E_{\mathrm{cut}}/k_B \sim 60$ K. Indeed, the difference in acoustic bandwidth between Si diamond and Ba_8Si_{46} results in a Debye temperature that is altered by one order of magnitude, thus going far beyond the $N^{1/3}$ scaling of the crystal complexity factor.

Using this reformulated Debye temperature in semiempirical descriptions of thermal conductivity, such as the above-discussed approach by Madsen *et al.* [38], would thus allow to better capture the underlying physics of clathrates. Both the reduction of the acoustic bandwidth and the fact that most of the heat is found to be carried by acoustic phonons validate the development of further model approaches, allowing for developing large-scale Hamiltonians where the lattice dynamics is considered only in a reduced energy range [33].

To conclude, we have presented a systematic computational study of the lattice dynamics in Ba_xSi_{46} using this system as a model to disentangle the different contributions responsible for the decreased lattice thermal conductivity in clathrates. Despite the fact that experiment and calculation show significant differences—especially at higher temperatures—we nevertheless think that our model system yields important insights into the mechanisms that are responsible for the low lattice thermal conductivity in clathrates. However, the discrepancies between experiment and simulation clearly point to additional contributions to the lattice thermal conductivity in clathrates, which currently are not accounted for. Most importantly, our findings indicate that evidenced variations of the lattice thermal conductivity, which are induced by changes in the electronic carrier concentration—as, e.g., found in $Ba_8Cu_xSi_{46-x}$ [42] and $Ba_8Al_xSi_{46-x}$ [43]—not only may be a result of electron-phonon scattering, but also may originate in the changed interaction potential of the Si framework as evidenced from our comparison of Si_{46} and charged-Si_{46}. Thus, in the optimization of the electronic configuration of the cages, both the electronic properties and the impact on the lattice thermal conductivity should be considered. This provides new directions for further improvements of thermoelectric properties and costs of clathrate materials by reducing the amount of Ba and optimizing the nature of the defects/dopants on the cage framework.

[1] M. Beekman, D. T. Morelli, and G. S. Nolas, Better thermoelectrics through glass-like crystals, Nature Mater. **14**, 1182 (2015).

[2] W. Qiu, X. Ke, L. Xi, L. Wu, J. Yang, and W. Zhang, "phonon" scattering beyond perturbation theory, Sci. China: Phys., Mech. Astron. **59**, 627001 (2016).

[3] E. S. Toberer, A. Zevalkink, and G. J. Snyder, Phonon engineering through crystal chemistry, J. Mater. Chem. **21**, 15843 (2011).

[4] G. J. Snyder and E. S. Toberer, Complex thermoelectric materials, Nature Mater. **7**, 105 (2008).

[5] J.-A. Dolyniuk, B. Owens-Baird, J. Wang, J. V. Zaikina, and K. Kovnir, Clathrate thermoelectrics, Mater. Sci. Eng., R **108**, 1 (2016).

[6] T. Takabatake, K. Suekuni, T. Nakayama, and E. Kaneshita, Phonon-glass electron-crystal thermoelectric clathrates: Experiments and theory, Rev. Mod. Phys. **86**, 669 (2014).

[7] S. Yamanaka, Silicon clathrates and carbon analogs: high pressure synthesis, structure, and superconductivity, Dalton Trans. **39**, 1885 (2010).

[8] T. F. T. Cerqueira, S. Pailhès, R. Debord, V. M. Giordano, R. Viennois, J. Shi, S. Botti, and M. A. L. Marques, Prediction and synthesis of a non-zintl silicon clathrate, Chem. Mater. **28**, 3711 (2016).

[9] R. Castillo, W. Schnelle, M. Bobnar, U. Burkhardt, B. Böhme, M. Baitinger, U. Schwarz, and Y. Grin, The clathrate $Ba_{8-x}Si_{46}$ revisited: Preparation routes, electrical and thermal transport properties, Z. Anorg. Allg. Chem. **641**, 206 (2015).

[10] See Supplemental Material at http://link.aps.org/supplemental/10.1103/PhysRevB.97.014304 for theoretical background and calculation details. Moreover, dispersion curves, phonon density of states, participation ratio, and lattice thermal conductivity for further compounds are presented and analyzed.

[11] S. Pailhès, H. Euchner, V. M. Giordano, R. Debord, A. Assy, S. Gomès, A. Bosak, D. Machon, S. Paschen, and M. De Boissieu, Localization of Propagative Phonons in a Perfectly Crystalline Solid, Phys. Rev. Lett. **113**, 025506 (2014).

[12] H. Euchner, S. Pailhès, L. T. K. Nguyen, W. Assmus, F. Ritter, A. Haghighirad, Y. Grin, S. Paschen, and M. De Boissieu, Phononic filter effect of rattling phonons in the thermoelectric clathrate $Ba_8Ge_{40+x}Ni_{6-x}$, Phys. Rev. B **86**, 224303 (2012).

[13] P. Norouzzadeh, C W. Myles, and D. Vashaee, Phonon dynamics in type-viii silicon clathrates: Beyond the rattler concept, Phys. Rev. B **95**, 195206 (2017).

[14] M. M. Koza, M. R. Johnson, R. Viennois, H. Mutka, L. Girard, and D. Ravot, Breakdown of phonon glass paradigm in La- and Ce-filled Fe_4Sb_{12} skutterudites, Nature Mater. **7**, 805 (2008).

[15] Y. M. Beltukov, V. I. Kozub, and D. A. Parshin, Ioffe-Regel criterion and diffusion of vibrations in random lattices, Phys. Rev. B **87**, 134203 (2013).

[16] J. Hafner and M. Krajci, Propagating and confined vibrational excitations in quasicrystals, J. Phys.: Condens. Matter **5**, 2489 (1993).

[17] M. de Boissieu, R. Currat, S. Francoual, and E. Kats, Sound-mode broadening in quasicrystals: A simple phenomenological model, Phys. Rev. B **69**, 054205 (2004).

[18] M. de Boissieu, S. Francoual, M. Mihalkovic, K. Shibata, A. Q. R. Baron, Y. Sidis, T. Ishimasa, D. Wu, T. Lograsso, L-P. Regnault, F. Gähler, S. Tsutsui, B. Hennion, P. Bastie, T. J. Sato, H. Takakura, R. Currat, and A-P. Tsai, Lattice dynamics of the Zn-Mg-Sc icosahedral quasicrystal and its Zn-Sc periodic 1/1 approximant, Nature Mater. **6**, 977 (2007).

[19] A. Bodapati, P. K. Schelling, S. R. Phillpot, and P. Keblinski, Vibrations and thermal transport in nanocrystalline silicon, Phys. Rev. B **74**, 245207 (2006).

[20] P.-F. Lory, S. Pailhès, V. M. Giordano, H. Euchner, H. D. Nguyen, R. Ramlau, H. Borrmann, M. Schmidt, M. Baitinger, M. Ikeda, P. Tomes, M. Mihalkovic, C. Allio, M. R. Johnson, H. Schober, Y. Sidis, F. Bourdarot, L. P. Regnault, J. Ollivier, S. Paschen, Y. Grin, and M. de Boissieu, Direct measurement of individual phonon lifetimes in the clathrate compound $Ba_{7.81}Ge_{40.67}Au_{5.33}$, Nat. Commun. **8**, 491 (2017)

[21] M. Roufosse and P. G. Klemens, Thermal conductivity of complex dielectric crystals, Phys. Rev. B **7**, 5379 (1973).

[22] G. A. Slack, Thermal conductivity of elements with complex lattices: B, P, S, Phys. Rev. **139**, A507 (1965).

[23] G. A. Slack, The thermal conductivity of nonmetallic crystals, Solid State Phys. **34**, 1 (1979).

[24] A. J. Minnich, Advances in the measurement and computation of thermal phonon transport properties, J. Phys.: Condens. Matter **27**, 053202 (2015).

[25] T. Tadano, Y. Gohda, and S. Tsuneyuki, Anharmonic force constants extracted from first-principles molecular dynamics: applications to heat transfer simulations, J. Phys.: Condens. Matter **26**, 225402 (2014).

[26] C. H. Lee, I. Hase, H. Sugawara, H. Yoshizawa, and H. Sato, Low-Lying Optical Phonon Modes in the Filled Skutterudite CeRu 4 Sb 12, J. Phys. Soc. Jpn. **75**, 123602 (2006).

[27] T. Tadano, Y. Gohda, and S. Tsuneyuki, Impact of Rattlers on Thermal Conductivity of a Thermoelectric Clathrate: A First-Principles Study, Phys. Rev. Lett. **114**, 095501 (2015).

[28] W. Li and N. Mingo, Ultralow lattice thermal conductivity of the fully filled skutterudite $YbFe_4Sb_{12}$ due to the flat avoided-crossing filler modes, Phys. Rev. B **91**, 144304 (2015).

[29] W. Li and N. Mingo, Thermal conductivity of fully filled skutterudites: Role of the filler, Phys. Rev. B **89**, 184304 (2014).

[30] A. San-Miguel and P. Toulemonde, High-pressure properties of group IV clathrates, High Press. Res. **25**, 159 (2005).

[31] M. M. Koza, M. R. Johnson, and H. Mutka, Vibrational dynamics of the type-I clathrate $Ba_8Zn_xGe_{46-x-y}\square_y$ (x=0, 2, 4, 6, 8), Phys. Rev. B **82**, 214301 (2010).

[32] E. Reny, A. San-Miguel, Y. Guyot, B. Masenelli, P. Mélinon, L. Saviot, S. Yamanaka, B. Champagnon, C. Cros, M. Pouchard, M. Borowski, and A. J. Dianoux, Vibrational modes in silicon clathrate compounds: A key to understanding superconductivity, Phys. Rev. B **66**, 014532 (2002).

[33] Y. Liu, Q. Xi, J. Zhou, T. Nakayama, and B. Li, Phonon-glass dynamics in thermoelectric clathrates, Phys. Rev. B **93**, 214305 (2016).

[34] Q. Xi, Z. Zhang, J. Chen, J. Zhou, T. Nakayama, and B. Li, Hopping processes explain linear rise in temperature of thermal conductivity in thermoelectric clathrates with off-center guest atoms, Phys. Rev. B **96**, 064306 (2017).

[35] M. Ikeda, H. Euchner, X. Yan, P. Tomes, A. Prokofiev, L. Prochaska, G. Lientschnig, R. Svagera, S. Hartmann, E. Gati, M. Lang, and S. Paschen, Kondo-like phonon scattering in thermoelectric clathrates, arXiv:1711.08627.

[36] V. J. Härkönen and A. J. Karttunen, Ab initio studies on the lattice thermal conductivity of silicon clathrate frameworks II and VIII, Phys. Rev. B **93**, 024307 (2016).

[37] J. Dong, O. F. Sankey, and C. W. Myles, Theoretical Study of the Lattice Thermal Conductivity in Ge Framework Semiconductors, Phys. Rev. Lett. **86**, 2361 (2001).

[38] G. K. H. Madsen, A. Katre, and C. Bera, Calculating the thermal conductivity of the silicon clathrates using the quasi-harmonic approximation, Phys. Status Solidi A **213**, 802 (2016).

[39] C. Candolfi, U. Aydemir, A. Ormeci, M. Baitinger, N. Oeschler, F. Steglich, and Y. Grin, Low-temperature magnetic, galvanomagnetic, and thermoelectric properties of the type-i clathrates $Ba_8Ni_xSi_{46-x}$, Phys. Rev. B **83**, 205102 (2011).

[40] U. Aydemir, C. Candolfi, A. Ormeci, Y. Oztan, M. Baitinger, N. Oeschler, F. Steglich, and Yu. Grin, Low-temperature thermoelectric, galvanomagnetic, and thermodynamic properties of the type-i clathrate $Ba_8Au_xSi_{46-x}$, Phys. Rev. B **84**, 195137 (2011).

[41] C. Candolfi, U. Aydemir, M. Baitinger, N. Oeschler, F. Steglich, and Yu. Grin, High temperature thermoelectric properties of the type-i clathrate $Ba_8Au_xSi_{46-x}$, J. Appl. Phys. **111**, 043706 (2012).

[42] X. Yan, M. X. Chen, S. Laumann, E. Bauer, P. Rogl, R. Podloucky, and S. Paschen, Thermoelectric properties of Ba-Cu-Si clathrates, Phys. Rev. B **85**, 165127 (2012).

[43] N. Tsujii, J. H. Roudebush, A. Zevalkink, C. A. Cox-Uvarov, G. J. Snyder, and S. M. Kauzlarich, Phase stability and chemical composition dependence of the thermoelectric properties of the type-i clathrate $Ba_8Al_xSi_{46-x}$ ($8 \leqslant x \leqslant 15$), J. Solid State Chem. **184**, 1293 (2011).

[44] D. Schopf, H. Euchner, and H.-R. Trebin, Effective potentials for simulations of the thermal conductivity of type-I semiconductor clathrate systems, Phys. Rev. B **89**, 214306 (2014).